Synthesis and Characterization of Nanocast Silica NCS-1 with CMK-3 as a Template

An-Hui Lu, Wolfgang Schmidt, Bernd Spliethoff, and Ferdi Schüth*[a]

Abstract: Nanocast silica (NCS-1) was synthesized by a casting process by employing the mesoporous carbon CMK-3 (the replica of SBA-15) as a template, tetraethoxysilane (TEOS) as the silica source, and hydrochloric acid (HCl) as the catalyst. The ordered carbon template was removed by employing different methods, such as calcination, thermal treatment followed by calcination, and controlled combustion. According to XRD and TEM characterization, NCS-1 exhibits an ordered structure with hexagonal symmetry and retains the morphology of the original SBA-15 used for the synthesis of CMK-3 over two replication steps on the nanometer scale. This demonstrates the well-connected porosity in CMK-3 type carbon, which can be used as a mold to synthesize mesostructured materials. The nitrogen adsorption isotherms generally show type IV shape, indicating mesoporous characteristics. The structure of NCS-1 is strongly influenced by variables of the nanocasting process, such as the loading amount of silica, hydrolysis temperature, and carbon removal methods. The surface area, pore size, and pore volume of NCS-1 can be tuned to a certain range by varying these parameters.

Keywords: adsorption · mesoporous materials · nanocasting · scanning probe microscopy

Introduction

Since the synthesis of M41S materials in 1992,[1] mesoporous materials have attracted much attention, because such materials are promising for applications in heterogeneous catalysis, adsorption, low-*k* dielectrics, and many others. A number of studies have been carried out to find novel synthesis strategies to produce mesoporous solids.[2,3] The replication of nanostructures by using mesoporous silica as a template seems promising for synthesizing mesoporous materials by means of a nanocasting process.[4,5] For instance, mesoporous carbon, CMK-1, with a $I4_1/a$ (or lower) symmetry was first templated by MCM-48.[4] Later on, CMK-3, with a *p6mm* symmetry, was synthesized by replication of SBA-15.[6] Such processes rely on the fact that an ordered-pore system, provided by ordered mesoporous silicas, can be filled with a carbon precursor that can be pyrolyzed, and the silica leached with solutions of sodium hydroxide (NaOH) or hydrofluoric acid (HF). Details of the synthesis have been described in a recent review.[7] However, it is difficult to synthesize framework compositions other than carbon with this technique, as the leaching of the silica also typically affects the framework of other materials that are filled into the silica pore system. As an alternative, one could take the nanocasting approach one step further, as it is much easier to remove carbon than silica; namely by combustion, but in principle by other techniques also, such as reaction with sulfur, hydrogenation, or fluorination. Thus, ordered mesoporous carbon might be used as a mold for the synthesis of any material in a mesoporous and ordered form, as long as its precursors can be infiltrated into the pore system of carbon, and the material retains its integrity during carbon combustion.[8] Previous research of our group has practically verified this principle by the synthesis of nanocast silica No. 1 (NCS-1) using mesoporous carbon CMK-3 (the replica of SBA-15) as a template, by means of a repeated nanocasting process.[9,10] Also, independently, Kang et al. have demonstrated the feasibility of this approach, using a different silica precursor and also SBA-15 as the mold.[11] This synthetic strategy was recently extended to synthesize structured silica HUM-1 by using mesoporous carbon templated from MCM-48.[12] Moreover, a mesoporous carbon template has another advantage, that is, its high thermal stability and chemical inertness. This should also allow the accommodation of structural transformations of the infiltrated materials during the heat treatment. Domen and co-workers[13] have exploited this property in a slightly different way: they filled the pores of an amorphous niobium tantalum oxide with carbon, crystallized the oxide by treatment

[a] Dr. A.-H. Lu, Dr. W. Schmidt, B. Spliethoff, Prof. Dr. F. Schüth
Max-Planck-Institut für Kohlenforschung
Kaiser-Wilhelm-Platz 1
45470 Mülheim (Germany)
Fax: (+49) 208-306-2995
E-mail: schueth@mpi-muelheim.mpg.de

 DOI: 10.1002/chem.200400180

at high temperature in inert gas, and then removed the carbon by calcination.

In the initial communication we only demonstrated the possibility of repeated nanocasting as a proof of principle. Dependence of the characteristics of the synthesized silica on preparation parameters was only briefly addressed.[9] This will be described in more detail in this work, in which the structure of NCS-1, synthesized under different conditions, was investigated in order to thoroughly understand this method. The results obtained not only allow insight into the formation of silica cast on CMK-3 materials, but can also be transferred to other carbon templates, for example, carbon aerogels and xerogels, other CMK materials, or activated carbons, allowing the formation of completely new hierarchically ordered porous silicas.

Results and Discussion

Mesoporous silica (NCS-1) can be successfully synthesized by using a repeated nanocasting process, as we have demonstrated earlier.[9] Figure 1 shows the morphologies of the

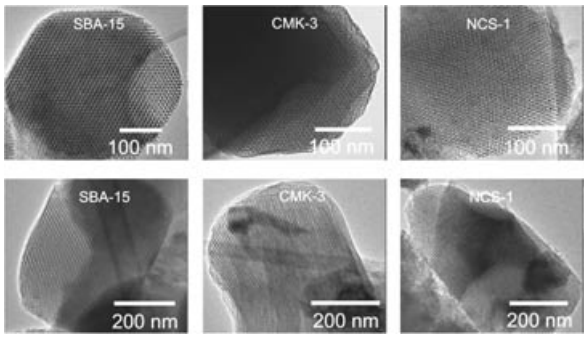

Figure 1. TEM observations of the morphologies of SBA-15, CMK-3, and the resultant NCS-1.

starting SBA-15, CMK-3 from this SBA-15, and NCS-1 from this CMK-3. The images show how the morphology and porosity of the particles is retained during the nanocasting process. This template method opens a novel synthetic pathway and probably can be applied to other types of metal oxides and even sulfides. For this purpose, it is necessary to clearly understand the influence of some important variables on structural properties.

Silica precursor and hydrolysis temperature: Experimental details of all variables are listed in Table 1 for the samples studied in this work. In the present study, TEOS was used as the silica source, because of its moderate hydrolysis rate and high ratio between the central silicon atom and the hydrolyzable groups.[9] In general, TEOS can be used for infiltration as-received, because of its liquid state and low viscosity. However, for other silica precursors dissolution may be necessary. Therefore we studied the dilution of TEOS with the precursor trimethylbenzene (TMB) and investigated the effect of the dilution. For these experiments, an aqueous HCl solution with pH 1 was used as a catalyst to initiate the hydrolysis of TEOS in the pore system of CMK-3. However, it should be pointed out that the infiltration sequence of TEOS and HCl influences the structure of the final product. When small amounts of HCl were introduced, and subsequently the TEOS was infiltrated into the CMK-3, even visually, small white spots could be identified on the CMK-3 particles, indicating inefficient infiltration of silica into the pore system of CMK-3. This is probably caused by premature hydrolysis of the TEOS and would lead to partial blocking of the pores from further infiltration. Hence, all further experiments were carried out using the sequence of firstly introducing TEOS and then HCl; this sequence was then repeated until the desired loading was achieved.

The samples NCS-1-1 and NCS-1-2 were obtained by using TEOS dissolved in TMB as the silica precursor. As can be seen in Figure 2, both samples exhibit an XRD reflection pattern with a very weak (100) peak, indicating a relatively disordered structure compared to other samples synthesized by directly using TEOS without dilution. Nitrogen adsorption measurements show that the two materials have very similar isotherms (Figure 3) with a clear hysteresis in the relative pressure range of 0.65–0.85, indicating that these samples are mesoporous. However, NCS-1-1 adsorbed substantially more nitrogen at low relative pressures, leading to a parallel shift of the isotherm. As in the low-pressure range micropores predominantly contribute to the adsorption, the difference between the two samples is mainly ascribed to the influence of the micropores that result from

Table 1. Typical experiments carried out for the study of the nanocasting process.

Samples	SiO_2 precursor	Hydrolysis temperature [°C]	SiO_2/C mass ratio	Removal of carbon template[a] A [°C]	B [°C]	C [°C]
composite 1	TEOS	40	0.4			
composite 2	TEOS	40	1.4			
NCS-1-1	TEOS+TMB	40	1.6		550	
NCS-1-2	TEOS+TMB	40	1.6	700/500		
NCS-1-3	TEOS	90	2.1			550
NCS-1-4	TEOS	90	2.1		550	
NCS-1-5	TEOS	40	1.9			550
NCS-1-6	TEOS	40	2.1		550	
NCS-1-7	TEOS	40	0.4	700/550		
NCS-1-8	TEOS	40	0.6			550
NCS-1-9	TEOS	40	0.9			550
NCS-1-10	TEOS	40	1.3			550
NCS-1-11	TEOS	40	1.7			550
NCS-1-12	TEOS	40	1.4	700/550		
NCS-1-13	TEOS	40	1.4		550	
NCS-1-14	TEOS	40	1.3	700/550		
NCS-1-15	TEOS	40	1.3	900/550		
NCS-1-16	TEOS	40	1.3	1100/550		

[a] A: Thermal treatment and calcination, B: calcination, C: controlled combustion.

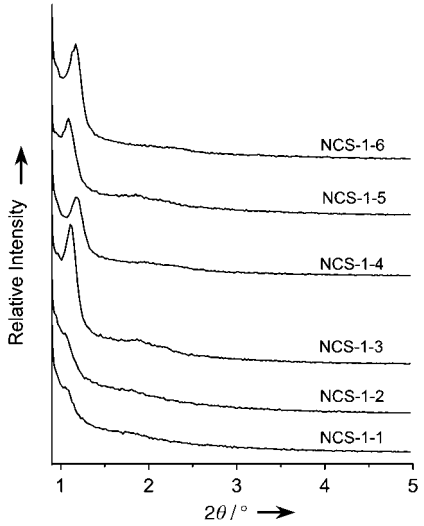

Figure 2. XRD patterns of NCS-1-1 to NCS-1-6.

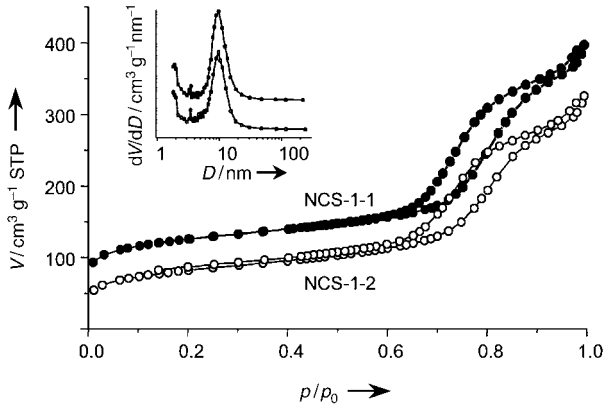

Figure 3. Nitrogen sorption isotherms of NCS-1 samples synthesized using TEOS and TMB as the silica source. The inset shows the pore size distributions.

the different template-removal methods. This will be discussed in more detail below. As expected from the very similar isotherms at higher relative pressures, NCS-1-1 and NCS-1-2 have almost identical pore size distributions (PSDs) as calculated by the BJH (BJH = Barrett–Joyner–Halenda) formalism, with a maximum pore diameter of about 10 nm (see the inset in Figure 3).

If perfect casting occurs, NCS-1 should not have pores as large as 10 nm, because these pores result from the combustion of the carbon rods forming the CMK-3 network. These rods have sizes around 7 nm, comparable to the size of the pores of the starting SBA-15 material. By ignoring the shrinkage of NCS-1 during the combustion step, the maximum pore size it could reach would thus be roughly 7 nm. To explore how the larger pores are formed if TEOS dissolved in TMB is used as the silica precursor, NCS-1-1 was also analyzed by TEM. As presented in Figure 4a and b, it can be clearly seen that NCS-1-1 is composed of ordered silica as usual with a hexagonal structure, as well as some disordered silica on the outer surface of the particle. This disordered silica results in decreased intensity of the XRD

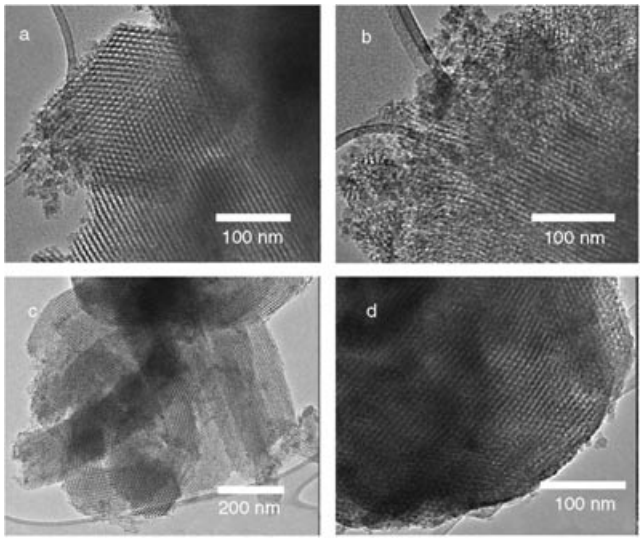

Figure 4. TEM images of NCS-1 samples synthesized by using TEOS dissolved in TMB (a and b: NCS-1-1) or TEOS in its undiluted form (c and d: NCS-1-12).

reflections and the relatively wide pore size distribution, with the maximum shifted to larger pore sizes. In contrast to this, TEM images of NCS-1-12 synthesized by using TEOS without TMB in Figure 4c and d (discussed in detail later) show well-developed pore structures; only minute amounts of disordered silica can be observed on the outer surface of NCS-1-12. Based on these TEM observations, we concluded that the pore size distributions of NCS-1-1 and NCS-1-2 obtained from the BJH calculation are average diameters of the pores generated both from the replica of CMK-3 and the disordered silica. These different pores cannot be distinguished by nitrogen adsorption. Thus, the use of TMB solvent leads to the formation of disordered silica on the outer surfaces of NCS-1 particles, and a mixture of materials with ordered and disordered structures is consequently obtained. It therefore seems advisable to use the silica precursor in as high a concentration as possible, ideally in its undiluted form.

It is well known that the hydrolysis temperature of TEOS determines its hydrolysis rate.[14] The higher the temperature, the faster the hydrolysis rate will be. In the present study, complete hydrolysis of the TEOS, infiltrated into the limited mesopore space of CMK-3, without evaporation was highly desired in order to form NCS-1 with a stable structure. Therefore, a compromise had to be found: the hydrolysis temperature should not be so high as to cause evaporation of TEOS from the mesopores to the outer surface, but hydrolysis should be sufficiently rapid to allow a reasonable processing speed. Therefore, two hydrolysis temperatures were investigated, namely, 40 °C and 90 °C. NCS-1-3 and NCS-1-4 were hydrolyzed at 90 °C and show a distinct (100) reflection in their XRD patterns (Figure 2). These properties do not strongly deviate for NCS-1-5 and NCS-1-6, hydrolyzed at 40 °C, as shown in Figure 2 and Table 2. This indicates that an ordered structure with hexagonal symmetry was formed in all of these samples. Therefore, the hydrolysis temperature does not strongly influence the ordered struc-

Table 2. Textural parameters of NCS-1 series.

Samples	S_{BET}[a] [$m^2 g^{-1}$]	V_{micro}[b] [$cm^3 g^{-1}$]	S_{meso}[c] [$m^2 g^{-1}$]	V_{single}[d] [$cm^3 g^{-1}$]	D_{BJH}[e] [nm]	a [nm]	t_{wall}[f] [nm]
Al/SBA-15	676	0.05	482	1.0	7.2	–	–
CMK-3	1043	0.09	867	0.90	3.8	–	–
NCS-1-1	432	0.103	181	0.57	10.0	–	–
NCS-1-2	290	0.041	172	0.50	10.0	–	–
NCS-1-3	541	0.105	262	0.46	5.4	9.6	4.3
NCS-1-4	449	0.089	196	0.31	4.2	8.6	4.4
NCS-1-5	557	0.084	327	0.49	4.9	9.4	4.1
NCS-1-6	541	0.110	232	0.37	4.2	8.7	4.9

[a] S_{BET}: specific surface area calculated based on the BET theory. [b] V_{micro}: micropore volume calculated from the *t*-plot method. [c] S_{meso}: mesopore surface area calculated by the BJH method (in p/p_0 range of hysteresis loop). [d] V_{single}: single-point total pore volume. [e] D_{BJH}: average pore diameter calculated from the BJH method (adsorption branch). [f] t_{wall}: wall thickness.

ture formation of NCS-1. However, it should be noted that some evaporation takes place at 90 °C and, therefore, impregnation of samples hydrolyzed at 90 °C needs to be repeated 2–3 times more than samples hydrolyzed at 40 °C to achieve the same silica loading of the CMK-3.

Loading amount of silica in CMK-3: After the general conditions for the optimal impregnating procedure had been established, the two factors that were assumed to be the key steps in controlling the structures of the resulting NCS-1 were studied, that is, the degree of loading of the CMK-3 and the carbon-removal procedure. The loading of CMK-3 with silica is the key factor in achieving NCS-1 with a stable structure. Due to the hydrolysis and condensation of TEOS, a substantial part of the pore is occupied by a mixture of water and ethanol. Therefore, it is impossible to fill the pore system of CMK-3 completely with silica by single step impregnation. Different loading amounts of silica in CMK-3 were obtained by repeating the impregnation procedure. The number of loading cycles was varied between two and six.

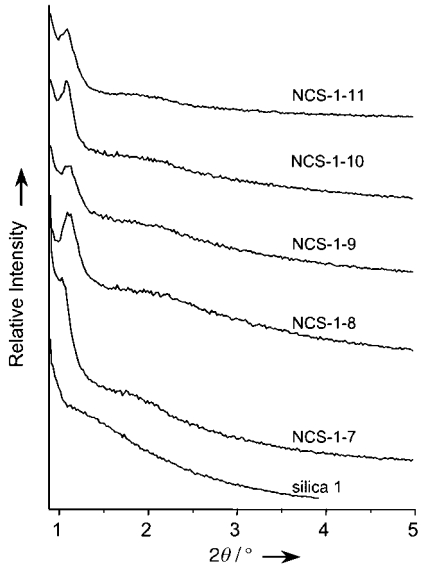

Figure 5. XRD patterns of NCS-1-7 to NCS-1-11 (SiO_2/C ratio $\geq$ 0.4). The sample denoted as "silica 1" has an SiO_2/C ratio below 0.4.

At a SiO_2/C ratio of about 0.4, the obtained NCS-1-7 shows only a weakly developed XRD pattern (Figure 5). The nitrogen adsorption isotherm (Figure 6) demonstrates the presence of a pore system in the size range of mesopores, with a relatively narrow pore size distribution (not shown here). At a SiO_2/C ratio below 0.4, the resultant NCS-1 does not show any XRD reflection in the low-angle range. One such sample is displayed in Figure 5, denoted as "silica 1". This indicates that the removal of the carbon template leads to a collapse of the silica mesostructure due to the low amount of silica present in the CMK-3, resulting in the formation of a disordered structure. At such a low silica loading, probably no coherent silica framework is formed, so that the structure loses its integrity after carbon removal.

As shown in Figure 6, with increasing SiO_2/C ratio from 0.6 to 1.7, the nitrogen adsorption isotherms of the as-prepared NCS-1-8 to NCS-1-11 still maintain type IV shape and are characteristic for mesoporous silica. However, the amount adsorbed decreases gradually; this is also reflected in a decrease of the specific surface area and of the pore volume (Table 3). Generally, the pore size of NCS-1 is related to the carbon wall thickness of the parent CMK-3. By

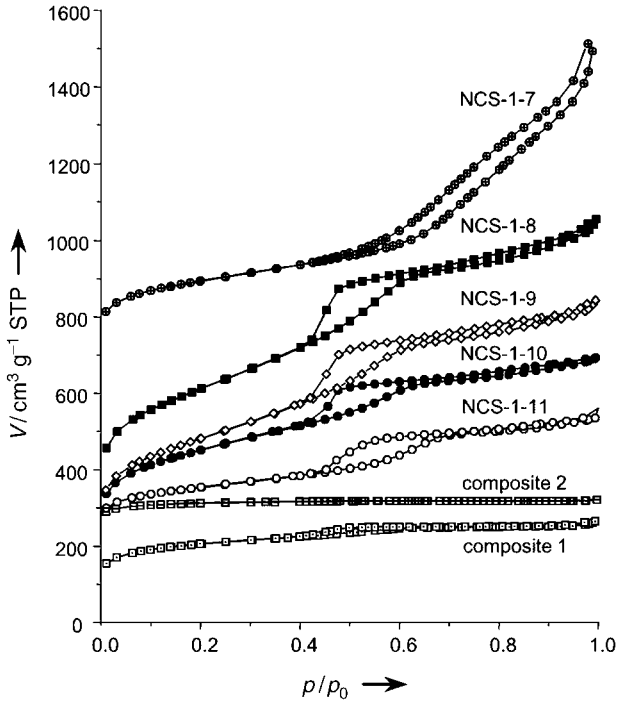

Figure 6. Nitrogen sorption isotherms of NCS-1 samples and their composites. The isotherm of composite 2 was offset vertically by 200 $cm^3 g^{-1}$ STP. From NCS-1-7 to NCS-1-11, the isotherms were offset vertically by 700, 300, 200, 200, and 200 $cm^3 g^{-1}$ STP, respectively.

Table 3. Textural parameters of NCS-1 series.

Samples	S_{BET}[a] [$m^2 g^{-1}$]	V_{micro}[b] [$cm^3 g^{-1}$]	S_{meso}[c] [$m^2 g^{-1}$]	V_{single}[d] [$cm^3 g^{-1}$]	D_{BJH}[e] [nm]	a [nm]	t_{wall}[f] [nm]
composite 1	706	0.178	199	0.40	3.5	–	–
composite 2	388	0.134	46	0.19	2.8	–	–
NCS-1-7	693	0.054	505	1.10	9.6	9.9	3.3
NCS-1-8	1151	–	1071	1.12	4.1	9.2	4.8
NCS-1-9	1030	–	900	0.95	4.1	9.3	5.0
NCS-1-10	909	0.014	659	0.75	3.9	9.4	4.7
NCS-1-11	537	0.065	347	0.51	4.8	9.4	4.0

[a] S_{BET}: specific surface area calculated based on the BET theory. [b] V_{micro}: micropore volume calculated from the *t*-plot method. [c] S_{meso}: mesopore surface area calculated by the BJH method (in p/p_0 range of hysteresis loop). [d] V_{single}: single-point total pore volume. [e] D_{BJH}: average pore diameter calculated from the BJH method (adsorption branch). [f] t_{wall}: wall thickness.

using the same CMK-3, it is expected that NCS-1 with a similar pore size can be prepared, assuming that its structure does not change during the carbon combustion. As seen in Figure 7, the maximum of the PSD moves to larger pore

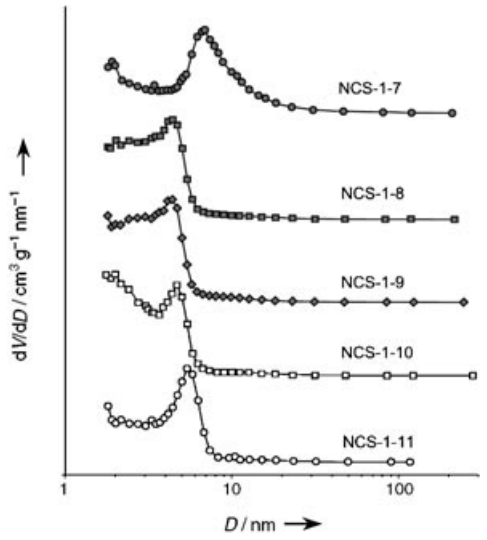

Figure 7. Pore size distributions of NCS-1-7 to NCS-1-11.

sizes with increasing SiO_2/C ratio, but is below 6.1 nm, the carbon-rod thickness of CMK-3. Moreover, the unit cell parameter *a* of NCS-1 is smaller than that observed for CMK-3 (10 nm) and exhibits a slight increase with increasing SiO_2/C ratio. These results indicate that the structure of NCS-1 shrinks to some extent during the combustion. With higher silica loadings, more stable structures of NCS-1 are obtained as the textural parameters are much closer to those of the mother template CMK-3. From Table 3 one can see that the micropore volume increases with increasing loading. This seems to be counterintuitive at first, since one would expect a more open silica framework for lower loadings and thus higher micropore volume. However, as stated above, the less filled materials show stronger shrinkage, which most probably leads to the loss of microporosity, unlike the highly loaded samples, in which the microporosity is maintained. One should keep in mind, however, that the determination of the micropore volume by the *t*-plot method is not very precise for these samples; for the low-loaded samples, negative intercepts with the volume axis are observed, indicating that the reference isotherm (fully hydroxylated silica) is not fully appropriate.

The effect of the loading amount of silica in CMK-3 can actually be best studied in the silica–carbon composite samples before carbon combustion. The nitrogen adsorption isotherms of the composites treated at 700 °C under nitrogen are also shown in Figure 6. When the SiO_2/C ratio is about 0.4 (composite 1), a hysteresis in the isotherms can be clearly seen, indicating that the mesopores of CMK-3 are not completely filled with silica at such low loading. However, when the SiO_2/C ratio reaches about 1.4 (composite 2) the hysteresis vanishes, and the mesopores of CMK-3 are almost completely filled. All of the composites exhibit a sharp increase in the volume adsorbed at the very beginning of the isotherms below $p/p_0 = 0.05$, indicating that a high micropore volume is created by the infiltration of silica. The textural data in Table 3 clearly show that the micropore volume of the composite is as high as $0.18\ cm^3 g^{-1}$. These observations for the composites corroborate the conclusions drawn above for the resulting NCS-1 materials. Microporosity is present initially, but due to the shrinkage during the carbon combustion the microporosity is lost, except for the more stable, highly loaded samples.

Removal of carbon template: As mentioned in the previous communication,[9] the structure of NCS-1 is strongly influenced by the different methods used to remove the carbon template. The removal of the carbon was performed here by three different pathways: A) thermal treatment in inert gas and subsequent calcination, B) simple calcination, and C) controlled combustion. The detailed information is listed in Table 1.

NCS-1-12 was obtained by the treatment of the SiO_2/C composite according to method A. For comparison, the same composite was calcined directly, namely method B, to remove the carbon template, leading to the formation of NCS-1-13. As seen in Figure 8, NCS-1-12 exhibits a larger unit cell than NCS-1-13, due to the different template removal method. Thermal treatment leads to increased condensation of SiO_2 in the pore system of CMK-3; this in turn stabilizes the ordered silica structure and makes it less susceptible to shrinkage during the carbon combustion. The nitrogen adsorption isotherms presented in Figure 9 show that both NCS-1-12 and NCS-1-13 are typical mesoporous materials demonstrated by a clear hysteresis loop. Both samples exhibit a narrow pore size distribution, as shown in Figure 10. However, NCS-1-12 possesses a larger pore size than that of NCS-1-13. Again, this is attributed to the thermal treatment preventing the silica framework from significant shrinkage. The textural parameters listed in Table 4 show that NCS-1-12 has a lower BET surface area but simi-

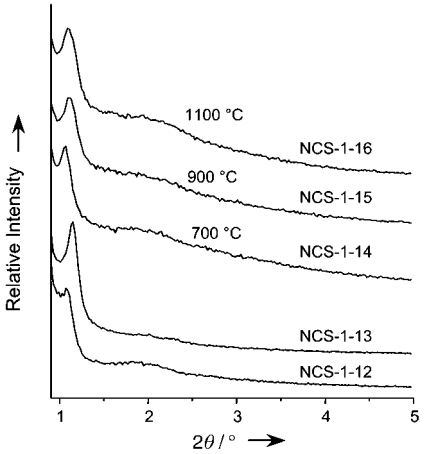

Figure 8. XRD patterns of NCS-1-12 to NCS-1-16.

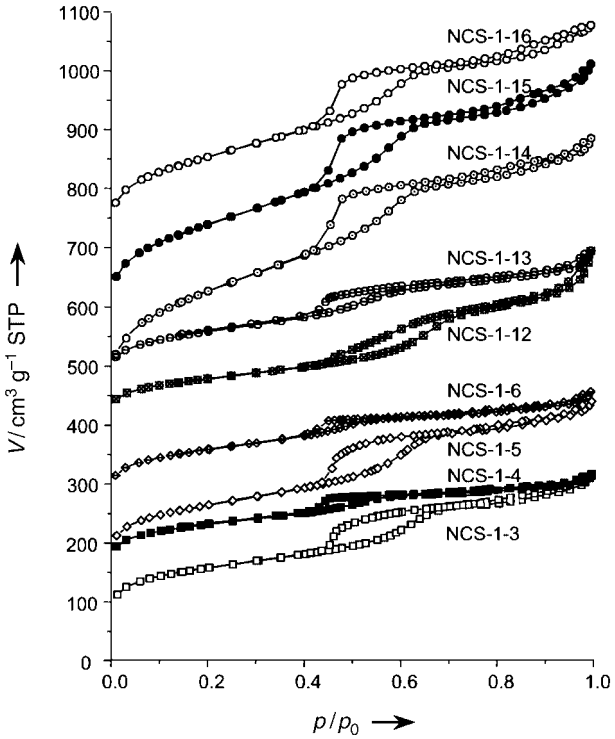

Figure 9. Nitrogen sorption isotherms of NCS-1. From NCS-1-4 to NCS-1-6, the isotherms were offset vertically by 100, 100, 200 $cm^3 g^{-1}$ STP, respectively. From NCS-1-12 to NCS-1-16, the isotherms were offset vertically by 400, 450, 400, 550 and 700 $cm^3 g^{-1}$ STP, respectively.

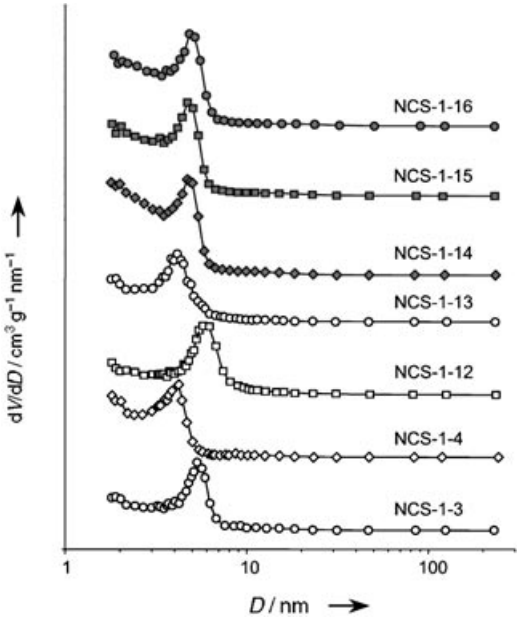

Figure 10. Pore size distributions of NCS-1-3, NCS-1-4, and NCS-1-12 to NCS-1-16.

lar mesopore surface area relative to those of NCS-1-13. The micropore volume of NCS-1-13 is much higher than that of NCS-1-12. This confirms that thermal treatment increases the condensation degree of silica in CMK-3 and in turn leads to the formation of a rigid silica skeleton, which does not shrink significantly during carbon combustion. Results from nitrogen adsorption isotherms agree well with the XRD data. The hexagonal order of the channels of NCS-1 is visible in the TEM images in many sections, as shown in Figures 4c and d. All sections of the sample show channels that are clearly similar to the ones present in SBA-15 (Figure 1); also clearly visible are the noodle-shaped particles, which are likewise often observed in SBA-15. The distance of 9 nm between channels observed in the TEM images corresponds well to the unit cell parameter calculated from the XRD pattern of sample NCS-1-12. The results show that the structure of CMK-3 is transferred into the silica imprint.

Removing the carbon template by methods B and C also have different influences on the final structure. For this series, samples with high silica loading were selected as examples. As seen before (Figure 2 and Table 2), NCS-1-3 and NCS-1-5, both treated according to method C, exhibit larger unit cells than those of samples NCS-1-4 and NCS-1-6, both treated with method B. Interestingly, the isotherm shape of the samples was related to the template removal method. As seen in Table 1 and Figure 9, the same template removal method leads to identically shaped isotherms; for instance, NCS-1-3 is similar to NCS-1-5, and NCS-1-4 is similar to NCS-1-6. The isotherms of samples NCS-1-3 and NCS-1-5 (Figure 9) show an evident hysteresis and cover a larger pressure range, as well as adsorbing a higher volume in the step, relative to those of samples calcined directly (NCS-1-4 and NCS-1-6). These differences are caused by the different carbon removal methods, with direct calcination resulting in significant structural shrinkage. To compare, NCS-1-5 has a lower micropore volume, but larger mesopore surface area than NCS-1-6, even though NCS-1-6 has a higher SiO_2/C ratio. This is in line with the notion that the controlled combustion causes additional condensation of silica. On the other hand, the BJH pore size distributions, as presented in Figure 10, clearly show that thermally pretreated samples (NCS-1-3 and NCS-1-5) have larger pore sizes than directly calcined samples (NCS-1-4 and NCS-1-6). Again, results from nitrogen adsorption isotherms and XRD are consistent with each other.

Moreover, the influence of a thermal pretreatment step at high temperature for method A was also investigated. The

Table 4. Textural parameters of NCS-1 series.

Samples	S_{BET}[a] [$m^2 g^{-1}$]	V_{micro}[b] [$cm^3 g^{-1}$]	S_{meso}[c] [$m^2 g^{-1}$]	V_{single}[d] [$cm^3 g^{-1}$]	D_{BJH}[e] [nm]	a [nm]	t_{wall}[f] [nm]
NCS-1-12	272	0.003	239	0.38	7.2	9.5	3.5
NCS-1-13	379	0.026	263	0.34	4.8	8.9	4.7
NCS-1-14	819	0.004	629	0.71	4.1	9.6	4.9
NCS-1-15	689	–	574	0.67	4.5	9.2	4.5
NCS-1-16	556	–	484	0.56	4.4	9.3	4.7

[a] S_{BET}: specific surface area calculated based on the BET theory. [b] V_{micro}: micropore volume calculated from the *t*-plot method. [c] S_{meso}: mesopore surface area calculated by the BJH method (in p/p_0 range of hysteresis loop). [d] V_{single}: single-point total pore volume. [e] D_{BJH}: average pore diameter calculated from the BJH method (adsorption branch). [f] t_{wall}: wall thickness.

composite was pretreated under nitrogen at either 700, 900, or 1100 °C, in order to achieve a high degree of silica condensation. Afterwards, the composite was calcined in a muffle oven following method A, leading to the formation of NCS-1-14, NCS-1-15, and NCS-1-16, respectively. The XRD pattern of NCS-1-14 (Figure 8) shows a large unit cell parameter *a*, indicating that the silica was sufficiently condensed to resist the shrinkage that could possibly be caused by carbon combustion. Samples NCS-1-15 and NCS-1-16 both have a similar unit cell parameter *a*; however, it is smaller than that of NCS-1-14, because of the structural shrinkage during the high-temperature treatment. This can be further verified by analyzing the nitrogen adsorption isotherms, as shown in Figure 9. All these samples exhibit a similar type IV isotherm with a clear condensation step in the middle relative pressure range, indicating mesoporous characteristics. As seen in Table 4, the higher the thermal treatment temperature, the lower the micropore content. Moreover, the mesopore surface area and the pore volume of NCS-1 treated at 700 °C are the highest and decrease with increasing thermal treatment temperature. These three samples exhibit a similar pore size with a maximum between 4 and 5 nm, indicating that the dominant pore size does not change with increased treatment temperature. This suggests that after annealing at temperatures of around 700 °C, complete condensation of the silica in CMK-3 occurs. A further increase of temperature does not lead to additional evident changes in the structures of the silica or the carbon.

The above analysis of results strongly demonstrates that the structure of NCS-1 depends greatly on the carbon-removal procedure. In turn, this also provides the opportunity for tailoring the structure of the NCS-1 obtained just by varying the processing conditions. In addition, it is noteworthy that NCS-1-16 treated at 1100 °C does not show any indication of the existence of silicon carbide according to the NMR analysis. This means silica and carbon do not react at 1100 °C under the present conditions, even though both of them are highly dispersed on the nanometer scale, at which high reactivity might have been expected.

Conclusions

The results presented show that it is possible to create a highly ordered mesoporous silica by repeated nanocasting with CMK-3-type carbon (the replica of SBA-15), which itself is obtained by nanocasting, as a mold. It is highly surprising that a true replication of the nanostructure can be achieved in repeated nanocasting steps. Figure 1 demonstrates how perfect the replication is. It is not only the mesostructure that is replicated, but also the general morphology of the SBA-15 is recovered in the NCS-1 samples. The optimum synthesis conditions consist of repeated impregnation/hydrolysis/condensation cycles with undiluted TEOS at 40 °C hydrolysis temperature. For template removal, simple calcination is the least favorable method, as the confining carbon framework is lost while condensation of silica still proceeds, thus resulting in a lower degree of order and loss of pore volume. Depending on the desired properties of the NCS-1 materials, thermal treatment in an inert atmosphere and subsequent calcination or controlled combustion are both suitable pathways for carbon removal. By adjustment of the processing conditions, the pore volume and the ratio between micropores and mesopores can be tailored to some extent.

For the synthesis of an ordered mesoporous silica, this pathway is rather complicated. Although the textural properties of the NCS-1 differ to some extent from the SBA-15 due to the processing at high temperatures, the generation of ordered silica following this pathway does not appear to be too attractive. However, the synthesis of the silica is prototypic and it is hoped that this process can be transferred to the synthesis of other base-metal and transition-metal oxides, possibly even sulfides or halogenides, because carbon can also be removed by reaction with sulfur at high temperature or with the more reactive halogens.

Experimental Section

The principal of the experimental procedure is represented in Scheme 1. Briefly, an ordered mesoporous silica, SBA-15, was impregnated with a precursor for carbon to obtain an ordered mesoporous carbon, known as CMK-3; after removal of the silica by aqueous HF treatment, this mesoporous carbon was then used as a new mold to produce another nanocast by impregnation with tetraethoxysilane. After calcination in air to remove the carbon, with an optional thermal treatment in inert atmosphere before calcination, another ordered mesoporous silica was obtained, denoted as NCS-1.

Synthesis of SBA-15: SBA-15 was synthesized by using Pluronics P_{123} as surfactant according to published procedures.[15] Tetraethoxysilane (8.5 g, 98 %, Aldrich) was hydrolyzed at 40 °C in water (105 mL) for 4 h in the presence of hydrochloric acid (20 mL, 37 %) and Pluronics P_{123} (4 g), and

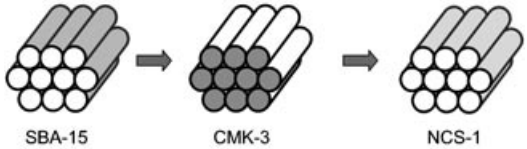

Scheme 1. Schematic illustration of the synthesis of NCS-1.

then aged at 80 °C for 24 h. The filtered sample was calcined at 550 °C for 5 h with a heating rate of 1 °C min^{-1} to obtain SBA-15. Furthermore, aluminosilicate SBA-15 (Al/SBA-15) was obtained through the following procedure: calcined SBA-15 (1 g) was impregnated by a solution of aluminum chloride ($AlCl_3$, 1 g) in ethanol (100 mL) under vigorous stirring for 14 h. The resulting Al/SBA-15 was filtered and washed with ethanol to remove the aluminum from the outer surface as much as possible, followed by a calcination step at 550 °C for 5 h in air.

Synthesis of CMK-3: Furfuryl alcohol (98 %, Fluka), as the carbon precursor, was introduced into the pores of Al/SBA-15 by incipient wetness impregnation, followed by carbonization of the infiltrated furfuryl alcohol. For this the sample was heated in nitrogen from 80–150 °C at a heating rate of 1 °C min^{-1}, kept at 150 °C for 3 h, then heated from 150 °C to 300 °C at a heating rate of 1 °C min^{-1}. Finally, the temperature was increased to 850 °C with a heating rate of 5 °C min^{-1} and kept at that temperature for 4 h. In general, by using 1 g of SBA-15, 2 g of composite can be obtained. To remove the silica, the composite (2 g) was treated in an aqueous HF solution (150 mL, 20 %). After filtration, washing with water, and drying steps, CMK-3 was obtained. The ash content of the sample was less than 0.5 %, thus demonstrating almost complete removal of the silica; this is important to check the success of the next step.

Synthesis of NCS-1: CMK-3 (0.5 g) was impregnated dropwise with TEOS (0.5 mL) under vigorous agitation. Then an aqueous solution of HCl (2–3 drops, pH 1) was added to initiate the hydrolysis of TEOS. This hydrolysis was carried out at different temperatures for 3 h. Subsequently, the water and ethanol formed were removed by evaporation at 80 °C. After removal of water and ethanol from the silica/carbon composite, the impregnation procedure was repeated until the desired amount of silica was reached. CMK-3 was removed by three different methods, which resulted in the formation of white powdery materials (NCS-1).

In order to investigate the influence of the variables affecting the final structural properties of NCS-1 generated from CMK-3, several important variables were chosen. Firstly, pure TEOS or TEOS diluted with trimethylbenzene was selected as the silica precursor. Subsequently, hydrolysis of these silica precursors was performed at either 40 °C or 90 °C, at different loading levels of silica ranging from 0.4 to 2.1 (denoted as SiO_2/C mass ratio). Finally, the carbon template was removed by three different methods: A) Thermal treatment and subsequent calcination. Normally, the composite was heat-treated up to 700 °C in a furnace under nitrogen in order to achieve a high degree of silica condensation, and then the composite was calcined in a muffle oven at 550 °C for 5 h; B) Calcination in air. The composite was heated to 550 °C in a muffle oven and calcined at that temperature for 5 h; C) Controlled combustion. The composite was heated to 550 °C in flowing nitrogen, then the gas was switched to air to burn out the carbon. The air-flow rate was controlled in order to keep the temperature of the sample below 550 °C, thus avoiding hot spots that could damage the structure of the forming silica. All of these methods resulted in the formation of white powdery materials. A survey of all the experiments carried out is presented in Table 1. It should be noted that the reproducibility of sample properties, such as pore volume, surface area, pore size, and lattice parameters, were typically found to be within 5 % based on the results obtained for many more samples than discussed here.

Characterization: Low-angle X-ray diffraction patterns were recorded with a Stoe STADI P diffractometer in Bragg–Brentano (reflection) geometry with $Cu_{K\alpha}$ radiation. The step width was 0.02° 2θ at an acquisition time of 8 s per step. Nitrogen adsorption isotherms were measured with an ASAP 2010 adsorption analyzer (Micromeritics) at liquid nitrogen temperature. Prior to the measurements, all samples were degassed at 250 °C for at least 3 h. The pore size distribution was calculated from the nitrogen adsorption isotherm by using the BJH method. The position of the maximum of the PSD was used to determine the pore diameter. All of the textural parameters of as-prepared samples are compiled in Tables 2–4, for which the micropore volume and mesopore surface area were calculated by using the *t*-plot method. The wall thickness of NCS-1, determined by subtraction of the pore diameter from the value of the unit cell parameter *a*, is also listed in these tables. TEM images of samples were obtained with a HF 2000 microscope (Hitachi) equipped with a cold field emission gun. The acceleration voltage was 200 kV.

Acknowledgements

Financial support by the DFG Leibniz Program and the FCI, in addition to the generous basic funding of the Max Planck Society, is gratefully acknowledged. A.-H. Lu would like to thank the Alexander von Humboldt Foundation for a fellowship.

[1] C. T. Kresge, M. E. Leonowicz, W. J. Roth, J. C. Vartuli, J. S. Beck, *Nature* **1992**, *359*, 710.
[2] J. Y. Ying, C. Mehnert, M. S. Wong, *Angew. Chem.* **1999**, *111*, 58; *Angew. Chem. Int. Ed.* **1999**, *38,* 56.
[3] F. Schüth, *Chem. Mater.* **2001**, *13*, 3184.
[4] R. Ryoo, S. H. Joo, S. Jun, *J. Phys. Chem. B* **1999**, *103*, 7743.
[5] A.-H. Lu, W. Schmidt, B. Spliethoff, F. Schüth, *Adv. Mater.* **2003**, *15*, 1602.
[6] S. Jun, S. H. Joo, R. Ryoo, M. Kruk, M. Jaroniec, Z. Liu, T. Ohsuna, O. Terasaki, *J. Am. Chem. Soc.* **2000**, *122*, 10712.
[7] R. Ryoo, S. H. Joo, M. Kruk, M. Jaroniec, *Adv. Mater.* **2001**, *13*, 677.
[8] F. Schüth, W. Schmidt, *Adv. Mater.* **2002**, *14*, 629.
[9] A.-H. Lu, W. Schmidt, A. Taguchi, B. Spliethoff, B. Tesche, F. Schüth, *Angew. Chem.* **2002**, *114*, 3639; *Angew. Chem. Int. Ed.* **2002**, *41*, 3489.
[10] F. Schüth, *Angew. Chem.* **2003**, *115*, 3730; *Angew. Chem. Int. Ed.* **2003**, *42*, 3604.
[11] M. Kang, S. H. Yi, H. I. Lee, J. E. Yie, J. M. Kim, *Chem. Commun.* **2002**, 1944.
[12] J. Y. Kim, S. B. Yoon, J. Yu, *Chem. Mater.* **2003**, *15*, 1932.
[13] T. Katou, B. Lee, D. Lu, J. N. Kondo, M. Hara, K. Domen, *Angew. Chem.* **2003**, *115*, 2484; *Angew. Chem. Int. Ed.* **2003**, *42*, 2382.
[14] C. J. Brinker, G. W. Scherer, *Sol-Gel Science: The Physics and Chemistry of Sol-Gel Processing*, Academic Press, New York, **1990**.
[15] D. Zhao, J. Feng, Q. Huo, N. Melosh, G. H. Fredrickson, B. F. Chmelka, G. D. Stucky, *Science* **1998**, *279*, 548.

Received: February 23, 2004
Revised: July 14, 2004
Published online: October 29, 2004

